Supporting Information for J. Phys. Chem. C, http://dx.doi.org/10.1021/jp210137u

Co-Catalytic Solid-State Reduction Applied to Carbon Nanotube Growth

Bernhard C. Bayer[1], Martin Fouquet[1], Raoul Blume[2], Christoph T. Wirth[1], Robert S. Weatherup[1], Ken Ogata[1], Axel Knop-Gericke[3], Robert Schlögl[3], Stephan Hofmann[1], John Robertson[1]

[1]Department of Engineering, University of Cambridge, Cambridge, CB3 0FA, UK
[2]Helmholtz-Center Berlin for Materials and Energy, D-12487 Berlin, Germany
[3]Fritz-Haber-Institute of the Max-Planck-Society, D-14195 Berlin-Dahlem, Germany

Experimental Methods (full)

Polished Si(1 0 0) wafer pieces (~0.5 x 0.5 cm) covered with a 200 nm thick thermally grown SiO_2 layer (for the remainder referred to as "SiO_2") were covered with Ta thin films of 100 nm, 20 nm, 3 nm, 2 nm and 0.5 nm thickness. Ta films were sputter deposited in a custom built DC-magnetron sputter coater from a Ta target (99.95%) at 30 W applied power and an Ar (99.9995%) pressure of $4x10^{-3}$ mbar (base pressure of system $1x10^{-5}$ mbar). Film thickness was checked by an in-situ quartz crystal balance and ex-situ spectroscopic ellipsometry (Woollam). The thickness of the 100 nm Ta films was checked by measuring the step height of during deposition partially covered samples by a profilometer (Dektak 11A).

Ta samples and, for reference, SiO_2 samples were then covered with Fe films of 0.5 nm, 1 nm and 3 nm in the same sputter deposition system and at the same conditions as the Ta films but with an applied power of 20 W. Again thickness was checked by an in-situ quartz microbalance as well as ex-situ spectroscopic ellipsometry. Note that thickness values refer to metal thicknesses and the film thickness increases upon exposure to ambient air due to oxide formation. We estimate an uncertainty of ± 30% to all stated thickness values, apart from the Ta 100 nm films which have an estimated uncertainty of ± 10 nm.

Low- and medium-pressure chemical vapor deposition (CVD) of carbon nanotubes (CNT) was carried out, after transfer and storage of samples in ambient air, in a custom-built, reduced pressure CVD chamber. The system was pumped with a turbo pump (base pressure of $1x10^{-6}$ mbar) for low pressure CVD and by a rotary pump (base pressure of $1x10^{-3}$ mbar) for medium pressure CVD, respectively. Samples were heated on a resistively heated boron-nitride coated graphite heater and gases (C_2H_2 (99.6%), NH_3 (99.999%), H_2 (99.9995%) and Ar (99.9995%)) were introduced via a showerhead ~5 cm from the samples. The processing conditions are summarized in Table 1. Temperatures were measured by a thermocouple attached to the heater and crosschecked by a pyrometer. We estimate an uncertainty of ± 50ºC in our stated temperature readings.

In-situ XPS analysis was performed at the BESSY II synchrotron in the ISISS end station of the FHI-MPG where samples were loaded after transport in ambient air into a reaction cell via a load lock and placed in front of a differentially pumped lens system of a hemispherical analyzer (Phoibos 150, SPECS) ~1.3 mm away from the aperture. A focused infrared laser was used for heating the sample from the outside through a view port. Temperatures were measured by a thermocouple clamped to the sample and, as such, an underestimation of up to ~100 °C may have occurred. The CVD atmosphere, controlled by Mass-Flow-Controllers (Bronkhorst) was constantly monitored by a mass spectrometer (Prisma Balzers) attached via a leak valve. For further details on the apparatus see ref. S1.

The in-situ XPS spectra shown here were collected in gas atmosphere (low pressure CVD conditions as indicated in Table 1) as well as in vacuum in normal emission geometry at photon energies of 435 eV (C1s), 1030 eV (Fe2p), 830 eV (O1s) and 330eV eV (Ta4f) with a spectral resolution of ~0.3-0.4 eV. At these photon energies, the electron mean free path is ~7-15 Å. The analysis area was ~ 100 µm x 1 mm. Background correction was performed using a Shirley background. Spectra were fitted following the Levenberg-Marquardt algorithm to minimize the χ^2 value. Peak shapes were modeled using asymmetric Doniach-Sunjic functions convolved with Gaussian profiles [allowing for asymmetric peak shapes where necessary (metallic Ta, TaC and sp^2 carbon)]. Note that the O2s region overlaps with the Ta4f spectrum in the metallic region. Since the former peak is a broad feature at ~22.8 eV it was

subtracted together with the background for the Ta fits with metallic components in Figure 3.

The morphology of samples was characterized with a scanning electron microscope (SEM, FEI Philips XL30 sFEG) and a scanning transmission electron microscope (STEM) equipped with an energy dispersive X-ray (EDX) spectrometer (Hitachi S-5500). For STEM analysis nanotubes and nanoparticles were transferred onto Au TEM-grids by scratching them off the wafers. The crystalline quality of the CNTs was assessed by Raman spectroscopy (Renishaw Raman spectrometer, 514.5 nm excitation).

Supporting Figures

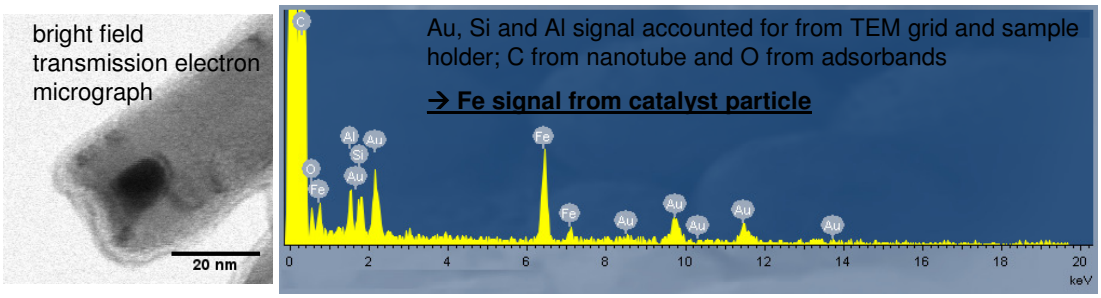

Supporting Figure 1: (left) Exemplary Bright-Field STEM micrograph of a nanoparticle at the root of a nanotube (low pressure CVD, vacuum pre-treatment followed by pure C_2H_2 growth, ~620 ºC, Fe 1 nm/Ta 2 nm) (right) Corresponding EDX spectrum of this particle, showing Au, Al, Si, C, O and Fe. With baseline EDX spectra taken away from any nanotubes the Au signal can be attributed to the Au-TEM grid and the Al and Si signals to the STEM sample holder. The C signal is from the nanotube, and O most likely from adsorbands, as confirmed by EDX scans of tube regions without visible metal particles. Thus the Fe signal in the spectrum can only be attributed to the catalyst particle in the image, confirming our assertion that Fe is the catalytically active species for CNT nucleation (while Ta in turn activates the Fe).

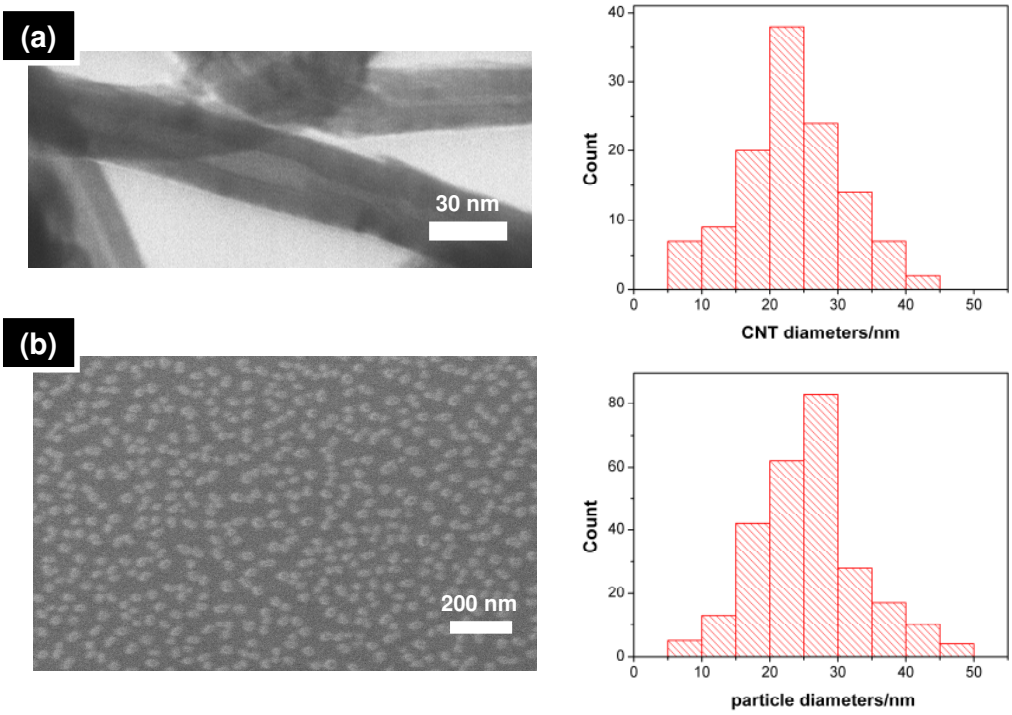

Supporting Figure 2: (a) (left) Scanning transmission electron micrograph of low pressure grown FeTa-catalyzed tubes (vacuum pre-treatment followed by pure C_2H_2 growth, ~620 ºC, Fe 1 nm/Ta 2 nm), showing multi-walled-type tubes. (right) Corresponding diameter distribution of nanotubes from these CVD conditions, mean ~23.5 nm. (b) (left) Scanning electron micrgraph of a low pressure vacuum annealed (~620 ºC) Fe 1nm/Ta 2 nm film. (right) Corresponding diameter distribution of the particles from these annealing conditions, mean ~25 nm. The nanotube diameters and nanoparticle diameters are in good agreement, where the small shift in the nanoparticles towards slightly larger values is attributed to oxidation effects (and hence volume expansion) of the nanoparticles during samples transfer in ambient air as well as catalyst reshaping dynamics during multi-wall CNT nucleation as in ref. S2.

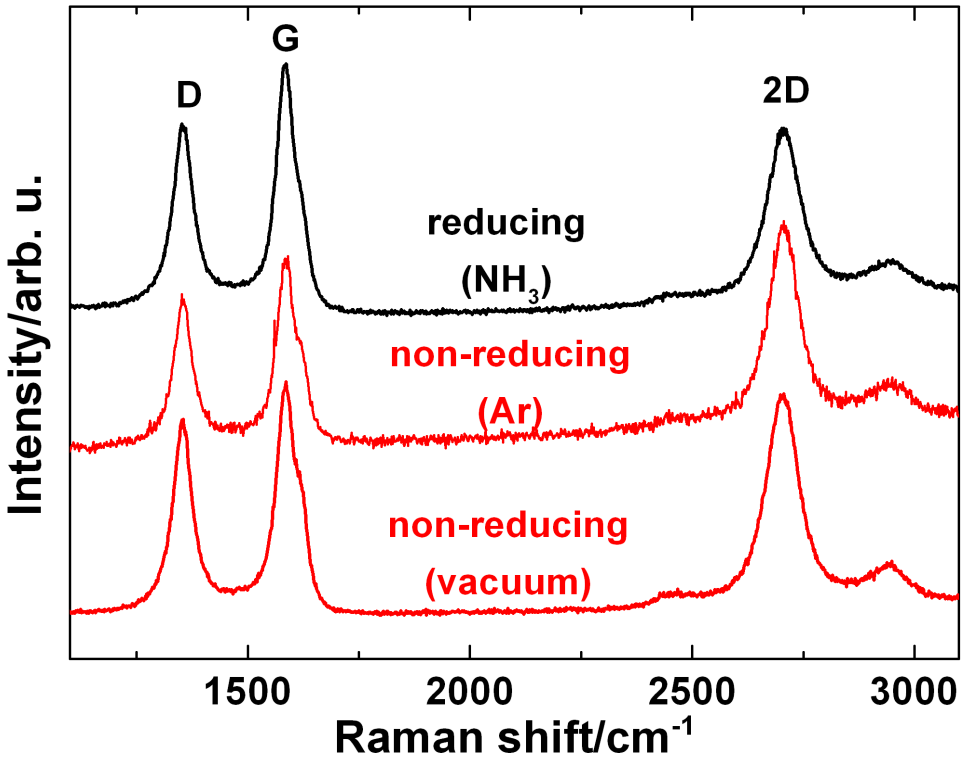

Supporting Figure 3: Raman spectra from typical growth from FeTa/SiO_2 (Fe ~1 nm/Ta ~2 nm) under low pressure CVD conditions at ~620 ºC with the reducing/non-reducing conditions indicated. Raman scans correspond to the SEM micrographs from Figure 2(a-c), column (ii).

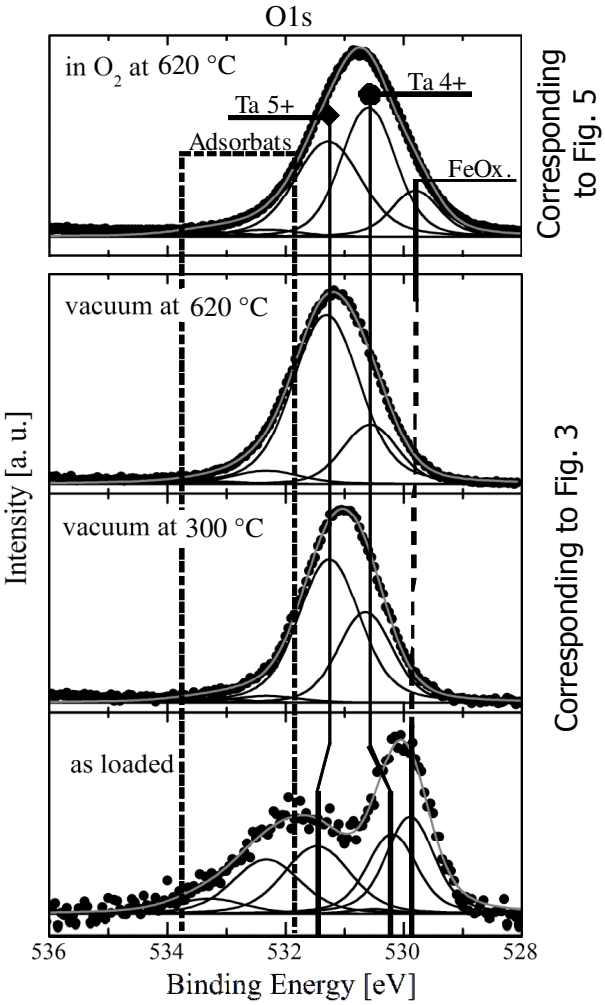

Supporting Figure 4: In-situ XPS O1s spectra of FeTa/SiO_2 as loaded, after vacuum annealing at 300 ºC and 620 ºC, and at 620 ºC in O_2 atmosphere ($4x10^{-2}$ mbar). The spectra correspond to Figure 3 and Figure 5 in the main text, as indicated. Next to an expected high fraction of adsorbats, the as loaded sample exhibits a strong peak at 529.85 eV, attributed to Fe oxide, and two further peaks at 530.2 eV and 531.46 eV. The latter peaks are assigned to Ta in mixed oxidation states. With annealing to 620°C in vacuum the Fe oxide peak and most of the contaminants vanish whereas the Ta related peaks shift to 530.56 and 531.3eV, respectively, corresponding to oxidation states of 4+ and 5+ and in keeping with the metal core level spectra.[S3,S4] In the spectrum of the reoxidized sample (top) again all three metal oxide components – Fe oxide, Ta^{4+} and Ta^{5+} – are observed reflecting the changes of the corresponding metal spectra. The de-convolution of the O1s spectra of Ta oxides is not well documented in the literature. Thus, our assignments of the Ta oxidation states in the O1s spectra are based on matching peak ratios in the Ta4f region. We note that the O1s peak at ~531 eV may also be partially related to the SiO_2 substrate under the Ta film, as we observe upon annealing the appearance of a small peak matching SiO_2 in the corresponding Si2p spectra (not shown). The kinetic energy of the photoelectrons was 150 eV with an information depth of ~0.7 nm.

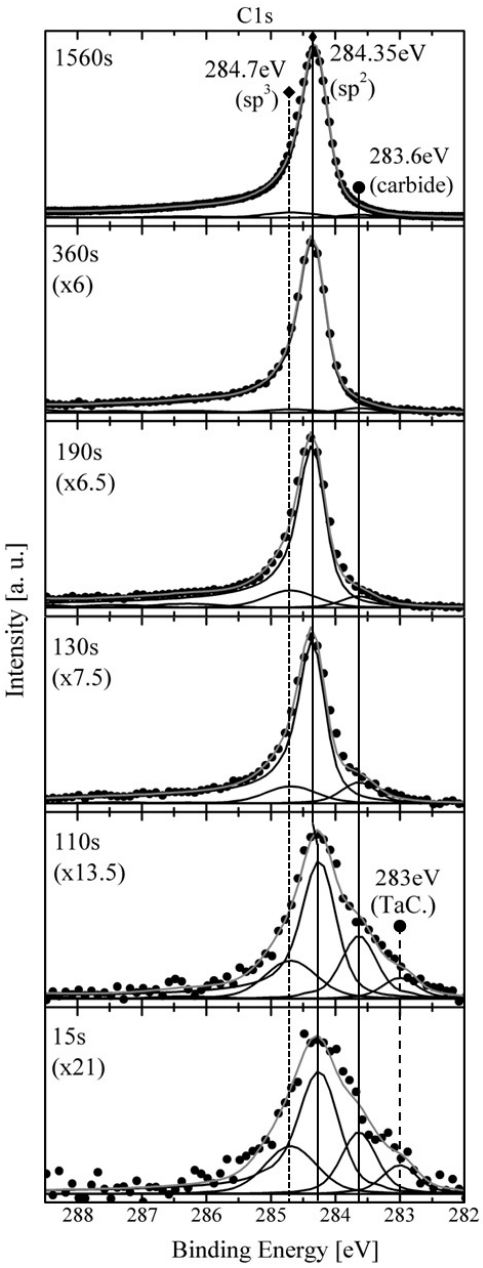

Supporting Figure 5: Time-resolved in-situ XPS C1s spectra of $FeTa/SiO_2$ after vacuum only pre-treatment i.e. when C_2H_2 is introduced at ~620 ºC. This corresponds to the next process step after Figure 3(b). The C1s evolution shows that after a short initial phase where sp^3 (284.7 eV) is formed, sp^2 carbon (284.35 eV) of high quality is grown.[S2,S5,S6] The kinetic energy of the photoelectrons was 130 eV corresponding to an information depth of ~0.7 nm.

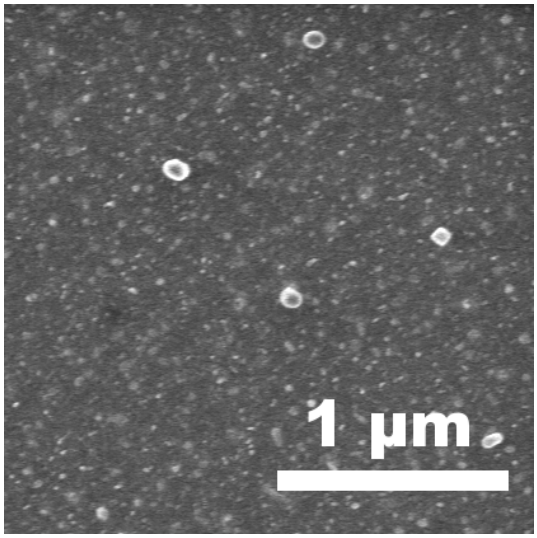

Supporting Figure 6: SEM micrograph of O_2 exposed ($4x10^{-2}$ mbar, ~620 °C) $FeTa/SiO_2$ after pre-treatment in vacuum and exposure to C_2H_2 at ~620 ºC. No tubes were grown in agreement with the deactivation of the Ta-sink mechanism and hence lack of reduction towards active, metallic Fe.

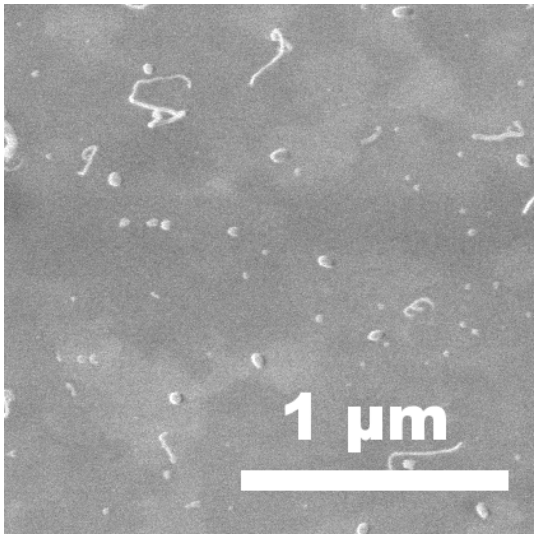

Supporting Figure 7: SEM micrograph of typical CNT growth from Fe/SiO_2 under low pressure, non-reducing vacuum conditions at ~620 ºC for C_2H_2 exposure times >60 min.

Supporting References

[S1] Knop-Gericke, A.; Kleimenov, E.; Hävecker, M.; Blume, R.; Teschner, D.; Zafeiratos, S.; Schlögl, R.; Bukhtiyarov, V. I.; Kaichev, V. V.; Prosvirin, I. P.; Nizovskii, A. I.; Bluhm, H.; Barinov, A.; Dudin, P.; Kiskinova, M. *Adv. Catal.* **2009**, *52*, 213-272.

[S2] Hofmann, S.; Sharma, R.; Ducati, C.; Du, G.; Mattevi, C.; Cepek, C.; Cantoro, M.; Pisana, S.; Parvez, A.; Cervantes-Sodi, F.; Ferrari, A. C.; Dunin-Borkowski, R.; Lizzit, S.; Petaccia, L.; Goldoni, A.; Robertson, J. *Nano Lett.* **2007**, *7*, 602-608.

[S3] E. Atanassova, E.; Tyuliev, G.; Paskaleva, A.; Spassov, D.; Kostov, K. *Appl. Surf. Sci.* **2004**, *225*, 86-99 and references therein.

[S4] Lecuyer, S.; A. Quernerais, A.; Jezequel, G.; *Surf. And Interf. Anal.* **1992**, *18*, 257-261.

[S5] Hofmann, S., Blume, R., Wirth, C. T., Cantoro, M., Sharma, R., Ducati, C., Haevecker, M., Zafeiratos, S., Schnoerch, P., Oesterreich, A., Teschner, D., Albrecht, M., Knop-Gericke, A., Schloegl, R., Robertson, J. *J. Phys. Chem. C.* **2009**, *113*, 1648-1656.

[S6] Mattevi, C.; Wirth, C. T.; Hofmann, S.; Blume, R.; Cantoro, M.; Ducati, C.; Cepek, C.; Knop-Gericke, A.; Milne, S.; Castellarin-Cudia, C.; Dolafi, S.; Goldoni, A.; Schloegl, R.; Robertson, J. *J. Phys. Chem. C* **2008**, *112*, 12207-12213.